Probing the cooperativity of *Thermoplasma acidophilum* proteasome core particle gating by NMR spectroscopy

Rui Huang[a,b,c], Felipe Pérez[a,b,c], and Lewis E. Kay[a,b,c,d,1]

[a]Department of Molecular Genetics, University of Toronto, Toronto, ON M5S 1A8, Canada; [b]Department of Biochemistry, University of Toronto, Toronto, ON M5S 1A8, Canada; [c]Department of Chemistry, University of Toronto, Toronto, ON M5S 1A8, Canada; and [d]Program in Molecular Medicine, Hospital for Sick Children, Toronto, ON M5G 1X8, Canada

Edited by Joseph D. Puglisi, Stanford University School of Medicine, Stanford, CA, and approved September 26, 2017 (received for review July 10, 2017)

The 20S proteasome core particle (20S CP) plays an integral role in cellular homeostasis by degrading proteins no longer required for function. The process is, in part, controlled via gating residues localized to the ends of the heptameric barrel-like CP structure that occlude substrate entry pores, preventing unregulated degradation of substrates that might otherwise enter the proteasome. Previously, we showed that the N-terminal residues of the α-subunits of the CP from the archaeon *Thermoplasma acidophilum* are arranged such that, on average, two of the seven termini are localized inside the lumen of the proteasome, thereby plugging the entry pore and functioning as a gate. However, the mechanism of gating remains unclear. Using solution NMR and a labeling procedure in which a series of mixed proteasome rings are prepared such that the percentage of gate-containing subunits is varied, we address the energetics of gating and establish whether gating is a cooperative process involving the concerted action of residues from more than a single protomer. Our results establish that the intrinsic probability of a gate entering the lumen favors the *in* state by close to 20-fold, that entry of each gate is noncooperative, with the number of gates that can be accommodated inside the lumen a function of the substrate entry pore size and the bulkiness of the gating residues. Insight into the origin of the high affinity for the *in* state is obtained from spin-relaxation experiments. More generally, our approach provides an avenue for dissecting interactions of individual protomers in homo-oligomeric complexes.

proteasome core particle | α_7 ring | proteasome gate | *in/out* gate conformation | methyl-TROSY

Cellular homeostasis is achieved, in part, through an intricate and highly regulated balance between protein synthesis and degradation (1, 2). Central to this balancing act is the proteasome, a supramolecular machine that is of vital importance for many aspects of cellular metabolism (3). The proteasome degrades misfolded or damaged proteins before they accumulate to a toxic level in the cell, produces antigenic peptides involved in the immune response, and plays a role in the cell cycle and in a variety of signal transduction events by regulating the concentrations of critical proteins in a timely manner (4–7). The importance of the proteasome is further underscored by the fact that it is recognized as an effective target for the development of a variety of inhibitors in the treatment of a number of malignancies and neurodegenerative disorders (8–10).

Detailed X-ray and cryo-EM studies have provided high-resolution pictures of the proteasome 20S core particle (20S CP) both in the free form and when bound to a number of adaptor molecules (11–21), including the 19S regulatory particle (19S RP) (18–21). The 20S CP is a barrel-shaped 670-kDa complex composed of four stacked heptameric rings arranged as α_7–β_7–β_7–α_7 that produces three interconnected chambers in the interior of the barrel. These include a central catalytic chamber that contains active site residues, and an antechamber on each side that maintains substrates in an unfolded state for hydrolysis (11, 22) (Fig. 1*A*). Substrate access to the sites of proteolysis, sequestered in the interior of the 20S CP, occurs via 13-Å-diameter gated pores at each end of the barrel structure (α-annulus) (Fig. 1 *B* and *C*). To ensure that proteins are only degraded when required, entry is controlled in a number of different ways. First, the 20S CP makes use of a gating mechanism whereby the N-terminal 10–15 residues of the α-subunits occlude the α-annulus, thereby regulating entry of substrates (12, 23). It has been shown in a series of in vitro studies using the 20S CP from the archaeon *Thermoplasma acidophilum* (*T. acidophilum* in what follows) that peptide substrate hydrolysis rates can be modulated by changing the extent to which the α-annulus is blocked by the gating residues (referred to in what follows as gates), with rates decreasing as the annulus becomes increasingly occluded (23). The importance of the 20S CP gates is further established through in vivo experiments showing that the viability of yeast decrease significantly under prolonged starvation when 20S CPs lack gating residues (24).

A second layer of regulation involves binding of the 20S CP to RPs that connect to the top and bottom of the CP barrel. Perhaps the most important of these in eukaryotes is the 19S RP that is composed of ∼20 protein components (4, 6). Binding of the 19S RP to the 20S CP protects against random protein degradation and ensures that only ubiquitylated proteins are recognized by the complex and degraded in a highly regulated and ATP-dependent manner that involves substrate threading into the 20S CP catalytic chamber. Other regulatory particles

Significance

In the cell, protein degradation occurs, to a large extent, by a barrel-like structure called the proteasome. Degradation is highly regulated, ensuring that only proteins targeted for elimination are removed. This is accomplished through gates that close the proteasome entrance pores, localized to the top and bottom of the structure, as well as through the binding of regulator molecules. Here, we study the properties of the individual gates using solution NMR spectroscopy and a labeling procedure in which a series of molecules are prepared with subunits that have different types of gates. Our results show that gates are formed via residues that have a very high intrinsic propensity to enter the lumen of the proteasome, with each gate behaving independently.

Author contributions: R.H. and L.E.K. designed research; R.H. and L.E.K. performed research; R.H. and F.P. contributed new reagents/analytic tools; R.H. and L.E.K. analyzed data; and R.H. and L.E.K. wrote the paper.

The authors declare no conflict of interest.

This article is a PNAS Direct Submission.

[1]To whom correspondence should be addressed. Email: kay@pound.med.utoronto.ca.

This article contains supporting information online at www.pnas.org/lookup/suppl/doi:10.1073/pnas.1712297114/-/DCSupplemental.

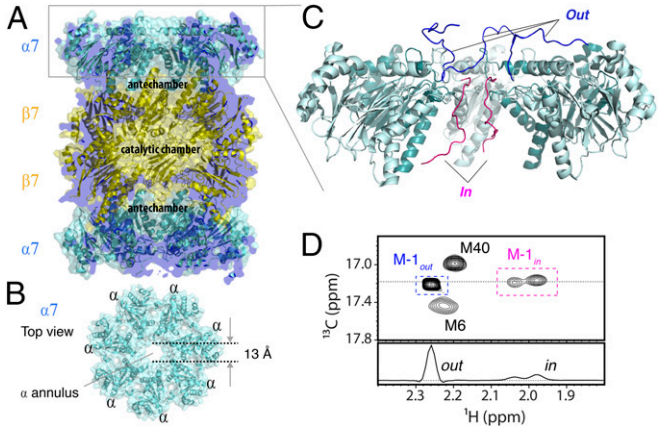

Fig. 1. Quantitation of *in*/*out* gate conformer populations in the α_7-ring from *T. acidophilium*. Side (*A*) and top (*B*) views of the 20S CP [Protein Data Bank (PDB) ID code 1YA7 (14)] showing the architecture of the four stacked rings ($\alpha_7\beta_7\beta_7\alpha_7$) (*A*) and the α-annulus at the entrance to the antechamber (*B*). Two front subunits are removed from each ring in *A* to show the antechambers and catalytic chamber in the interior of the CP. (*C*) Enlarged α_7-ring highlighting N-terminal gates that are either *in* (magenta) the antechamber or *out* (blue) [PDB ID code 2KU1 (23)]. (*D*) Selected region of the ^{13}C–^{1}H HMQC spectrum (800 MHz, 50 °C) of U-^{2}H, Met-[ε$^{13}CH_3$]–labeled PWT α_7-rings showing multiple correlations for the terminal methionine M-1, which are derived from the *in*/*out* conformations of the gates (23), with a 1D trace through the position of the dashed line (*Bottom*). The fractional population of the *in* conformation is 28.9 ± 0.8% based on ratios of cross-peaks for M-1 and corrected for differential relaxation effects (*Supporting Information*).

include the ATP-dependent unfoldases PAN and VAT in archaea (25, 26), the ATP-independent activator Bpa in bacteria (27), and PA28, PA200/Blm10 in eukaryotes (14, 28). PA28 is also known as the 11S RP and its binding to the proteasome enhances the hydrolysis of peptides but not of folded protein substrates (29). It has been shown that the binding of the 11S RP stabilizes the proteasome gates in an open conformation (14) and regulates the active sites of the 20S CP through an allosteric pathway (30).

In an effort to understand the mechanism of 20S CP proteasome gating in detail, we have used solution NMR spectroscopy that exploits a methyl-transverse relaxation optimized spectroscopy (TROSY) effect to improve spectral resolution and sensitivity in high–molecular-weight complexes and focused on methyl group probes of structure and dynamics (31, 32). The N-terminal α-subunit gating residues of the *T. acidophilum* proteasome were found to be highly dynamic and intrinsically disordered, yet the gates adopt distinct states in which they reside either inside the lumen of the antechamber (*in* conformation) or outside the antechamber above the α-ring (*out* conformation) (23) (Fig. 1*C*). The *in* and *out* conformations of the gates have lifetimes on the seconds timescale (23), and interconvert with a driving force that originates from random solvent motions (33). On average, two and five gates are in the *in* and *out* conformations, respectively, with the *in* gates penetrating the α-annulus and hence occluding the pore (23). In this manner, substrate entry is decreased. Although the conformations of the gates and their average equilibrium populations have been elucidated, important mechanistic questions remain. For example, it is not known whether the exchange between *in* and *out* gates is cooperative, what the intrinsic energetics are that govern the *in*/*out* equilibrium (i.e., probability of an individual gate entering the lumen), and how they are affected by the amino acid sequence of the gating residues. It is also not clear how the size of the annulus or the bulkiness of gating residues that cross the annulus affect the *in*/*out* thermodynamics. Moreover, since the seven gates of each α-ring are identical in the *T. acidophilum* 20S CP, it is of interest to establish whether the overall gating can be understood in terms of the behavior of an individual gate in this system.

Herein, we address these questions in the *T. acidophilum* 20S CP model system. NMR spectra in which each protomer is similarly labeled report on the average equilibrium distribution of *in* and *out* gates and cannot provide insight into the issue of gating cooperativity nor inform on the microscopic probabilities for a gate residing in the *in* or *out* state. We have therefore developed a labeling approach whereby heptameric α-rings are produced with variable numbers of gate-containing and gateless protomers, enabling properties of individual protomers to be elucidated. In this manner, we have been able to formulate a model that describes the *out*/*in* gating equilibrium in terms of parameters for individual gates. Our data are consistent with no cooperativity between adjacent gates and with an *in*/*out* probability that is very different from what might be naively assumed on the basis of cross-peak intensities in spectra where all protomers are identical. The gating sequence plays an important role in controlling *in*/*out* probabilities, with the α-annulus size influencing the number of gates in the *in* conformation under equilibrium conditions. Regions in the lumen of the proteasome barrel that influence the gating equilibrium have been established using paramagnetic relaxation enhancement NMR (34). Finally, the relative importance of intragate and intergate interactions in eliciting a change to the *in*/*out* gate population upon binding of the 11S activator to the proteasome has been established.

Results

An α_7 Model System. In previous studies of the proteasome, we have made use of a number of different constructs in addition to the 670-kDa 20S CP (22, 23, 35). These include both a single ring variant, α_7 (180 kDa), that contains seven copies of the α-protomer, as well as a double-ring variant, $\alpha_7\alpha_7$ (360 kDa), in which a pair of single α_7-rings stack on each other such that the annuli are at the top and bottom ends of the complex. Herein, we focus our studies on α_7, exploiting the improved spectral sensitivity and resolution in comparison with the 670-kDa 20S CP, although results are validated on the full complex. We have previously shown that the properties of the gating residues in the 20S CP proteasome are well reproduced in α_7 in terms of both the relative numbers of *in*/*out* gates and their intrinsic structural properties (23). We focus primarily on methyl group probes from Met residues since, of the five Met residues in the α-subunit, three are localized to the gates (M-1, M1, and M6). It has been previously shown that the cross-peaks derived from M-1 and M1 can be used as sensitive probes of the conformations of the proteasome gates (23); however, because M-1 and M1 overlap, complicating the accurate quantification of peak intensities that is essential to this study, we have engineered an M1I construct [referred to as pseudo–wild-type (PWT) in what follows]. For both the α_7-ring and the full 20S CP, the *in* and *out* conformations of the gating residues give rise to characteristic correlations in ^{13}C–^{1}H heteronuclear multiple-quantum correlation spectroscopy (HMQC) spectra of U-^{2}H, Met-[ε$^{13}CH_3$]–labeled protein (Fig. 1*D* and Fig. S1 *A* and *B*) that allow a direct estimate of the relative populations of each of the states using peaks derived from M-1 (Fig. 1*D*). Although a pair of peaks from M-1 are generated from the *in* state, as established previously via a combined mutagenesis and PRE study (23), the structural basis for the peak duplication is not understood presently. For PWT α_7-rings, the fractional population of the *in* gates is 28.9 ± 0.8%, corresponding to two gates localized inside the proteasome lumen on average, very similar to what is quantified for WT α_7-rings (29.4 ± 1.0%) (Fig. S1*A*) and for the WT 20S CP (29.0 ± 0.8%) (Fig. S1*B*). It is worth noting that populations are

obtained via cross-peak integration and include a correction for the differences in methyl ^{1}H transverse relaxation rates of magnetization derived from the *in* and *out* states (33), as described in *Supporting Information*.

The 20S Gates Have a High Intrinsic Probability to Adopt the *in* Conformation. The population of *in*/*out* gate conformers is influenced by several factors, including the intrinsic propensity for an individual gate to adopt the *in* conformation in the absence of gate–gate contacts (P^{in}), the pore size of the α-annulus that in turn dictates the maximum number of gates that can enter the lumen, M^{in}, and potential interactions between neighboring gates. Our previous NMR studies, confirmed presently (Fig. 1*D* and Fig. S1 *A* and *B*), show that two of seven gates in the WT proteasome are in the lumen on average. Naively, one might assume, therefore, that $P^{in} = 2/7$. Such an assumption is reasonable for the case where all configurations of gates are possible and when $M^{in} = 7$, yet the surface area of the annulus (Fig. 1*B*) cannot accommodate more than approximately three *in* gates. In this regard, a previous study showed that the proteasome can cleave circularized polypeptides (36), suggesting that at least two chains can enter simultaneously. To measure P^{in}, the steric hindrance caused by other *in* gates must be eliminated. Therefore, we constructed α_7-rings that were stochastic mixtures of protomers with and without the first 12 residues (Fig. S2) using an unfolding/refolding protocol described in *Supporting Information*. Only the PWT protomers were U-^{2}H, Met-[$\varepsilon^{13}CH_3$]–labeled (Fig. 2*A*, red spheres), while the gateless α-subunits (Δ1–12) were U-^{2}H (Fig. 2*A*, cyan spheres), mixed at a ratio of ∼1 to 20. Notably, the fractional populations of the *in*/*out* conformations of the gate shift significantly from 28.9 ± 0.8% *in* gates in PWT α_7-rings (Fig. 1*D*) to 95.4 ± 1.0% *in* for the predominantly gateless α_7-rings (Fig. 2*A*) that corresponds to a free-energy difference between *in*/*out* states, ΔG (*in* − *out*) of −1.9 kcal/mol. Very similar results were observed for predominately gateless α_7-rings reconstituted with ∼5% WT gate (94.0 ± 1.4% *in*) (Fig. S1*C*), as well as for the full 20S CP reconstituted in the same manner (96.0 ± 1.5% *in* gate) (Fig. S1*D*). Thus, the *T. acidophilum* proteasome gates have a high intrinsic propensity to adopt the *in* conformation, likely the result of favorable interactions between the *in* gate and the lumen of the chamber (see below).

The high P^{in} value may also reflect an absence of surrounding gates that could influence the equilibrium. To test this possibility, we first engineered a new gate that is enriched in Gly residues [MGGSEGGGSEGGGA (Fig. 2*B* purple spheres); compare with the PWT gate, MGIQQGQMAYDRAI]. Our choice of such a sequence was based on a desire to create a highly dynamic terminus that would potentially minimize interactions between gates from adjacent protomers by removing the Tyr residue (see below) and adding charge. A sample was prepared in which gateless α_7-rings (Fig. 2*B*, cyan spheres) were doped with ∼5% of Met-[$\varepsilon^{13}CH_3$]–labeled Gly-rich gate (Fig. 2*B*, purple spheres). In contrast to the case for α_7-rings that were predominately gateless and doped with PWT gates (Fig. 2*A*) where P^{in} = ∼95%, the Gly-rich gates adopt the *out* conformation (Fig. 2*B*), P^{in} < 5% [ΔG (*in* − *out*) ∼1.9 kcal/mol, corresponding to a $\Delta\Delta G$ of ∼4 kcal/mol for the *in*/*out* equilibrium relative to the PWT gates]. Thus, the intrinsic gate population distribution is significantly influenced by amino acid sequence. Having established that Gly-rich gates effectively do not penetrate the α-annulus (i.e., remain *out*), we next prepared α_7-rings that were predominately comprised of protomers with Gly-rich gates (∼95%, U-^{2}H; Fig. 2*C*, purple spheres) doped with U-^{2}H Met-[$\varepsilon^{13}CH_3$]–labeled α-subunits with PWT gates (∼5%, red spheres). Notably P^{in} = 95.6 ± 0.4% for the PWT gates, very similar to the value obtained in the gateless environment (95.4 ± 1.0%; Fig. 2*A*) and establishing that the Gly-rich gates above the annulus do not alter the intrinsic probability of gating termini entering the proteasome lumen. Thus, the high P^{in} value measured for the PWT gates is not the result of a lack of surrounding gates.

Gating Is Not Cooperative. Having established that there is a high probability for a PWT (or WT) gate to adopt the *in* conformation in the context of α_7-rings that are either predominately gateless or highly enriched in Gly-based gates (P^{in} = 95%; Fig. 2 *A* and *C*), we next sought to address the question of how cooperative the gating process might be. To this end, a titration experiment was performed in which mixed α_7-rings were reconstituted from U-^{2}H, Met-[$\varepsilon^{13}CH_3$]–labeled protomers with PWT gates and U-^{2}H–labeled gateless protomers using a range of different ratios of each type of protomer. Samples were made where the percentage of PWT gate-containing subunits varies from ∼5 to 100%. Notably, the percentage of *in* gates decreases as the proportion of gate-containing subunits that are incorporated into the α_7-rings increases, with 95.4 ± 1.0% and 28.9 ± 0.8% of gates in the *in* conformation as the fraction of PWT gates increases from ∼5% (Fig. 3*A*, left end, red circle, and *Inset* spectrum) to 100% (Fig. 3*A*, right end, magenta circle, and *Inset* spectrum). The distribution of *in*/*out*-labeled gates was fit to an initial model (see *Supporting Information*, *Model 1*) in which there is no explicit inclusion of interactions between adjacent gates, although the presence of interactions or lack thereof can often be inferred by the extracted probability values for successive gates adopting the *in* position. In this model, the probability of a gate entering the lumen depends only on the number of *in* gates (i.e., the number of gates that have already entered) and not on the number of *out* gates, nor on the relative position of either the *out* or *in* gates throughout the ring or on the number of gate-containing subunits.

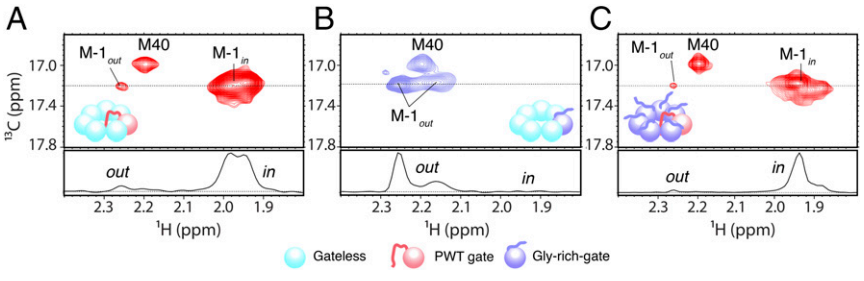

Fig. 2. PWT gates have a high intrinsic propensity of adopting the *in* conformation, P^{in}. (*A*) Selected region of an HMQC spectrum of α_7-rings reconstituted from ∼5% PWT gate (U-^{2}H, Met-[$\varepsilon^{13}CH_3$]–labeled, red sphere) and ∼95% gateless subunits (Δ1–12) (U-^{2}H, cyan spheres); a high percentage of *in* gates (95.4 ± 1.0%) is quantified. (*B*) As in *A* but for α_7-rings reconstituted with ∼5% Gly-rich gate-containing α-subunits (U-^{2}H, Met-[$\varepsilon^{13}CH_3$]–labeled, purple sphere) and ∼95% gateless α-subunits (U-^{2}H, cyan spheres). A very low percentage of *in* gates (<5%) is obtained. (*C*) Spectrum of reconstituted α_7-rings from 5% PWT gate-containing subunits (U-^{2}H, Met-[$\varepsilon^{13}CH_3$]–labeled, red sphere) and 95% Gly-rich gate-containing α-subunits (U-^{2}H, purple spheres) showing a high population of *in* gates (95.6 ± 0.4%). Primary sequences of the PWT gate and Gly-rich gate are MGIQQGQMAYDRAI and MGGSEGGGSEGGGA, respectively.

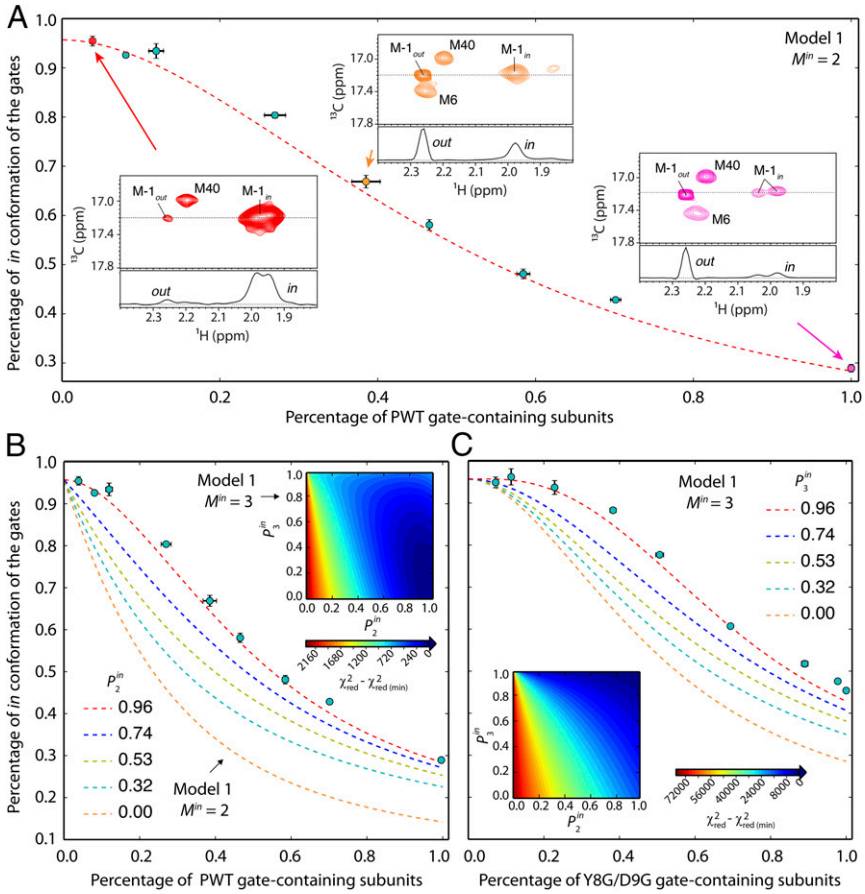

Fig. 3. Titration data are consistent with a lack of gating cooperativity. (*A*) Fractional population of *in* gates in a series of reconstituted α_7-rings comprising gateless subunits with an increasing proportion of PWT gate-containing subunits (circles). ^{13}C–^{1}H methyl HMQC spectra highlighting cross-peaks of M-1 at selected titration points are shown as *insets*. The dashed line is the fitted curve using a model assuming $M^{in} = 2$ and $P_1^{in} = P_2^{in} = P$, where P_1^{in} is the probability of the first gate entering the lumen and P_2^{in} is the probability of a second gate entering. The fitted value for P is 0.96 ± 0.01. (*B*) Titration curves simulated with $P_1^{in} = 0.96$ and P_2^{in} given as indicated, $M^{in} = 2$. (*C*) As in *A*, but where PWT gate-containing protomers are replaced with Y8G/D9G gate-containing subunits (circles). Titration curves are simulated with a model that assumes $M^{in} = 3$, $P_1^{in} = P_2^{in} = 0.96$, and P_3^{in} set to the values indicated and shown with dashed lines. *Insets* of *B* and *C* show χ^2_{red} as a function of P_2^{in} and P_3^{in} assuming $P_1^{in} = 0.96$ and $M^{in} = 3$ for titrations of PWT gate (*B*)- and Y8G/D9G gate (*C*)-containing subunits. Model 1 (*Supporting Information*) has been used in all of the analyses.

Interactions between gates in the *out* position are, thus, assumed to be negligible. A subsequent model (see below) removes this restriction. In the fits of the data of Fig. 3*A*, it is assumed that a maximum of two gating termini populate the proteasome lumen (i.e., $M^{in} = 2$) with the probabilities of the first and the second gate entering the lumen set to be the same, $P_1^{in} = P_2^{in} = P$. This corresponds to the case where gating is noncooperative. Note that, in the context of this model, positive cooperative gating occurs when $P_2^{in} > P_1^{in}$, that is, the presence of a gate inside the lumen leads to an increased probability of the second gate entering, while $P_2^{in} < P_1^{in}$ in the case of negative cooperativity. The best-fit value of P obtained is 0.96 ± 0.01 (Fig. 3 *A* and *B*, dashed red line). Notably, when the condition that $P_1^{in} = P_2^{in}$ is relaxed, we find that smaller P_2^{in} values do not produce acceptable fits of the data (Fig. 3*B*, dashed lines corresponding to $P_1^{in} = 0.96$, $0 \le P_2^{in} \le 0.74$), which rules out the possibility of negative cooperativity. Next, we considered the case where $P_1^{in} = 95.6\%$, as before, and $M^{in} = 3$, with P_2^{in} and P_3^{in} independent fitting parameters; best-fit values of 0.95 and 0.10 (Fig. 3*B*, *Inset*, and Fig. S3*A*) were obtained for P_2^{in} and P_3^{in}, respectively, suggesting that only two gates occupy the *in* position and that the presence of the first gate in the lumen does not influence the propensity of the second gate to enter subsequently. We have also performed fits where each of the P_i^{in} values is unrestrained and allowed to vary independently, and the same conclusions are obtained (Fig. S2*B*). Notably, in this case, P_2^{in} values are slightly larger than P_1^{in}, but the differences are small (0.95 ± 0.01 vs. 1.00 ± 0.03), and it remains the case that approximately equal probabilities are obtained. Although a nonzero population of the third *in* state appears to be optimal ($P_3^{in} \sim 0.1$ from the fit in Fig. 3*B*, *Inset*), it is small, corresponding to a free-energy penalty of 3.3 kcal/mol for gate entry relative to that obtained for the first gate ($P_1^{in} = 0.95$). Such small P^{in} values are sensitive to experimental errors, and we have shown that they vary by a few percent depending on the approach used to fit the data (Fig. S3).

Fits of the titration data of Fig. 3*A* are consistent with each gate acting in a noncooperative manner. Only when two gates are occupied in the proteasome antechamber does gate entry become prohibited because of steric constraints. To verify that gating does not depend on the *in*/*out* distribution of surrounding gates in this system but only on the number of gates in the *in* state, an assumption of the fitting model, we have refit the data in Fig. 3*A*. This was achieved by first dividing it into two subsets, corresponding to the first four points where the percentage of gate-containing subunits varies between ∼4% and ∼27% and the last four points where the corresponding fraction ranges from ∼50 to 100%. Each region of the curve was fit separately assuming $M^{in} = 2$ and $P_1^{in} = 95.6\%$. The similar values of P_2^{in}

obtained in both cases (>0.95), despite the fact that many more potential gating contacts could be made in α_7-particles containing a high fraction of PWT gates (second dataset), argues against interactions between gates in the *out* position that influence the *in*/*out* distribution.

We have carried out yet a further analysis to establish that gates from individual subunits are independent and that gating is noncooperative. As described in *Supporting Information*, a second model (*Model 2*) has been developed whereby the probability of a gate entering the lumen of the proteasome depends explicitly on whether the immediately adjacent protomer gates are in the *out* conformation. This model was motivated by X-ray crystal structures of a complex of the 11S RP and the proteasome, where the gates are all in the *out* state and interactions between gating residues on adjacent protomers were observed (14). Whether these contacts exist in the naked proteasome 20S CP in solution or, if they do, whether they contribute to gating is not known. Model 2 is very distinct from model 1 since the latter implicitly assumes that interactions in the *out* state are minimal by virtue of the assumption that P_i^{in} values depend only on the number of *in* gates and not on the number nor the distribution of *out* gates. Thus, if both models provide a set of consistent results, increased confidence in the gating mechanism can be obtained.

Fits of the titration data assuming model 2 and $M^{in} = 2$ establish that the probability of gate entry is independent of the state of the adjacent gates (*in* or *out*) since the obtained probability values for a gate entering the proteasome lumen are the same regardless of the orientation of the immediately surrounding gates (Fig. S4*A*). Although an excellent fit of the titration profile is obtained when $M^{in} = 2$, it is noteworthy that this model cannot fit the data assuming $M^{in} = 3$ (Fig. S4*B*). This reflects the fact (*i*) that effectively only two gates can reside in the lumen, consistent with the results from model 1 where a best fit value of 0.1 was obtained for P_3^{in} when P_1^{in} was fixed to 0.96 or a value of 0.05 when all P_i^{in} were allowed to float, and (*ii*) that unlike model 1 where $M^{in} = 3$, $P_3^{in} = 0$ reduces to $M^{in} = 2$, no such simplification is possible for model 2 (*Supporting Information*). Finally, it is worth noting that it is not possible to fit the data with model 2 in the limiting case where gating is assumed to be fully cooperative (Fig. S4 *A* and *B*, orange dashed lines), that is, where an adjacent protomer gate in the *out* position forces the gate in question to be *out*. In fact, none of the titration profiles reported here could be fit to such a scheme.

To explore how the size of the annulus in relation to the bulkiness of the residues that cross it influences gating, we next considered a Y8G/D9G mutant of the PWT gate and repeated the titration study described above in which an increasing proportion of Y8G/D9G gate-containing subunits (U-^{2}H, Met-[$\varepsilon^{13}CH_3$] labeled) was added to gateless α_7-protomers (U-^{2}H). Residues Y8 and D9 are proposed to stabilize the *out* gate conformation in the presence of the 11S RP (14, 23); however, it is not known what the effects of these mutations might be in the absence of RP binding. In contrast to WT or PWT α_7-rings, Y8G/D9G-rings have a higher percentage of *in* gates (45.4 ± 0.4%) (Fig. S5) that suggests a value of 3 for M^{in} (3/7 = 0.43) (23). Fig. 3*C* shows that the titration data (circles) for the Y8G/D9G mutant are well fit to model 1 with $M^{in} = 3$, $P_1^{in} = P_2^{in}$ set to 0.96, and P_3^{in}, a fitting parameter. Notably, the best fit is obtained with $P_3^{in} = 0.96$ (Fig. 3*C*, red dashed line), while smaller values of P_3^{in} fit much more poorly (Fig. 3*C*, dashed lines ranging from $0 \le P_3^{in} \le 0.74$). We have also fit the data to a model in which P_2^{in} and P_3^{in} are independent fitting parameters with the best fit obtained for $P_2^{in} \sim P_3^{in} \sim 1$ (Fig. 3*C*, *Inset*). The high-quality data fits using model 1, with essentially equivalent extracted P_i^{in} values, are consistent with individual gates functioning in an independent, noncooperative manner with regards to entry into the lumen of the proteasome barrel in the Y8G/D9G double mutant, as is the case for the PWT α_7-rings. We have also obtained an excellent fit using model 2 assuming that $M^{in} = 3$ (Fig. S4*C*). The extracted gating probabilities are again very similar, so that the probability of a gate entering the lumen does not depend on the up/down configurations of its immediate neighbors, consistent with a lack of gating cooperativity. As expected, there is a very poor correlation between the experimental titration curve and that predicted by model 2 when the condition of full gating cooperativity is imposed (Fig. S4*C*, orange dashed curve; see discussion in *Supporting Information*). The major difference between the Y8G/D9G and PWT gates is, therefore, that the glycine substitutions significantly increase the probability of a third gate adopting the *in* conformation. In this regard, it is noteworthy that structural models of the *T. acidophilum* α_7-gates based on paramagnetic relaxation enhancement (PRE) data show that the *in* gates cross the annulus in the region between residues A7 and R10 (23). Thus, the increased number of *in* gates relative to the PWT case (M^{in} of 3 vs. 2; compare Fig. 1*D* and Fig. S5) can be attributed to the smaller volume of Gly residues in relation to Tyr and Asp (37) and hence decreased steric clashes between individual Y8G/D9G gates upon penetrating the α-annulus, rather than to differences in gate–gate interactions in the WT and Y8G/D9G α_7-rings. The bulkiness of gate residues crossing the annulus in the present case or, in general, the size of the α-annulus thus plays an important role in dictating the number of gates that can be accommodated in the lumen.

Exploring the Origin of the High P^{in} Values. As described above, in the absence of steric hindrance, PWT (or WT) gates have a high propensity to adopt the *in* conformation. In an effort to obtain insight into what the driving factors might be for stabilizing the *in* state, we carried out a PRE study in which a nitroxide spin label was attached either to position −2 or 2 of the α-subunit, residues that are part of the gate. The unpaired electron of the spin label serves as a very efficient source of relaxation for surrounding NMR spins, leading to decreases in intensities of resonances in ^{13}C–^1H HMQC spectra in a manner that depends on the inverse sixth power of the distance of the electron to the nuclear spin in question (34). We have reconstituted α_7-rings in which protomers with spin labels are mixed with gateless α-subunits at a molar ratio of 1:4 (Fig. 4*A*, cartoon) so as to ensure that (*i*) the majority of the gates (~84%) adopt the *in* conformation and that (*ii*) most of the α_7-rings (~80%) have at least one gate per ring. Both gateless and gated subunits were highly deuterated and labeled as δ-[$^{13}CH_3$]-Ile, γ/δ-[$^{13}CH_3$,$^{12}CD_3$]-Val/Leu so that intraprotomer and interprotomer PREs are quantified. The PRE effect, given by the intensity ratio of a cross-peak before (I_{ox}) and after (I_{red}) the spin label is reduced, is plotted for each methyl probe in α_7 in Fig. 4*A* for the case where the spin label is attached at position −2 of the α-subunit. Residues that are significantly affected (I_{ox}/I_{red} more than 1 SD below the mean, indicated by the red dashed line in Fig. 4*A*) are located either on the gate (M-1 and M6) or inside the antechamber (V87, L88, V116, and V129), the positions of which are shown in Fig. 4*B* on a structure that omits the gates. Similar results were obtained when the spin label was attached to position 2 of the α-subunit (Fig. S6). Notably, the spin label at the 2 or −2 position has little effect on the populations of the *in*/*out* states, with values of 80% and 82% of *in* gates measured, respectively, from spectra of the reduced protein, close to what is expected when PWT gate-containing and gateless subunits are mixed in a 1:4 ratio (83.5%). The proximity between gating residue M1 in the *in* state and residue V129 that is located close to the α-annulus is confirmed by methyl–methyl nuclear Overhauser effects (NOEs) recorded on the WT α_7 (Fig. 4*C*). Interestingly, each of the methyl groups of V87, L88, and V129 gives rise to a pair of correlations in spectra recorded of the WT α_7-ring (Fig. 4 *D*–*G*, red single contour), while only a single peak is noted in spectra of Δ1–12 α_7 (Fig. 4 *D*–*G*, black contours). The multiplicity of peaks for the WT rings reflects the

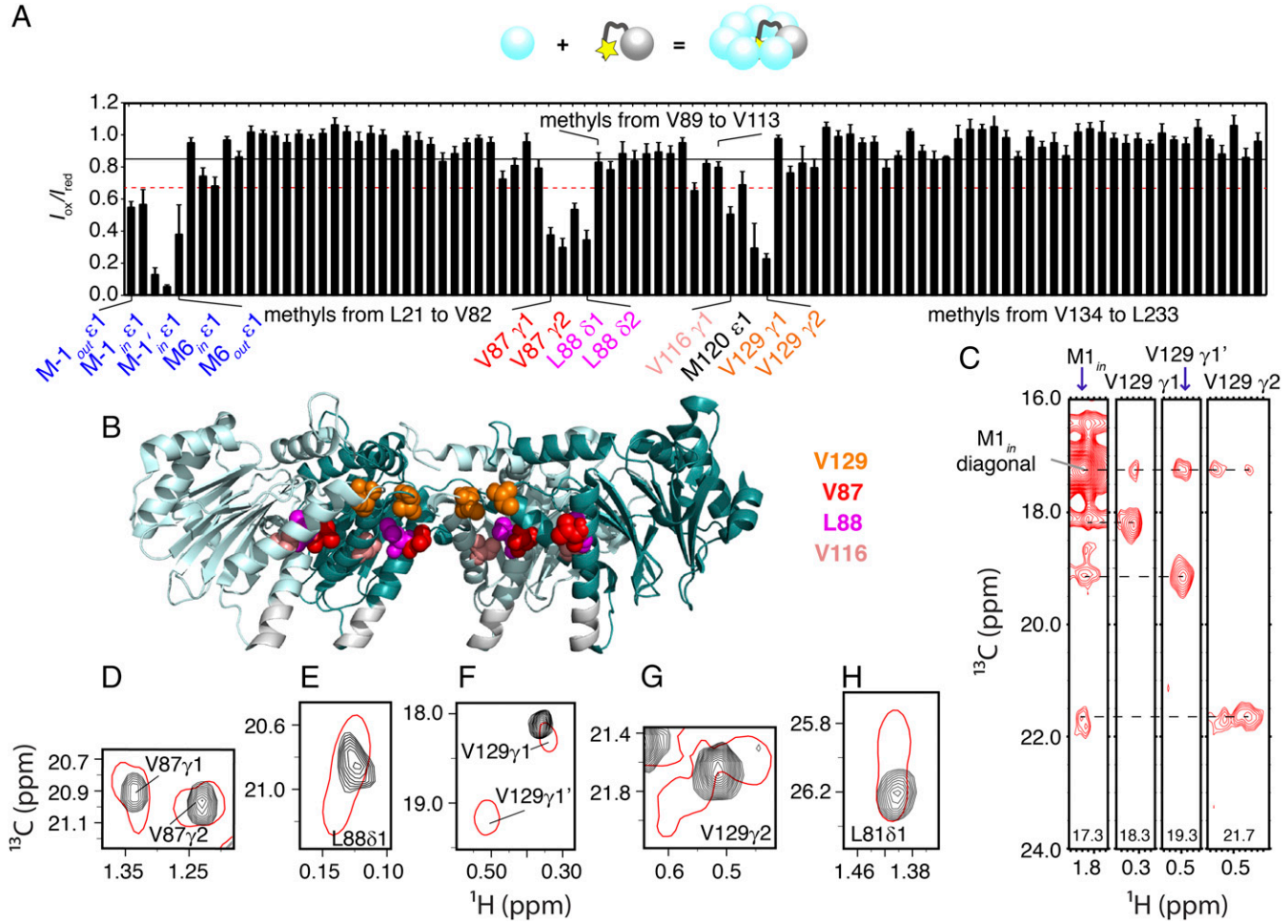

Fig. 4. Interactions between the *in* gates and the interior of the antechamber drive the *in* conformation. (*A*) PREs of methyl probes generated with a nitroxide spin label (yellow star) attached to position −2 of PWT gate-containing α-subunits (gray sphere); α_7-rings are reconstituted with 20% gate-containing subunits and 80% gateless subunits (cyan sphere). I_{ox}/I_{red} is the intensity ratio of a methyl correlation before (I_{ox}) and after (I_{red}) the spin label is reduced. The black (red) line denotes the average I_{ox}/I_{red} value (1 SD below average). Methyl groups with significant PREs (I_{ox}/I_{red} below the red dashed line) are labeled in color in *A*. The corresponding residues are located on the gate (M-1 and M6; note that there are two M-1 *in* peaks, denoted by M-1_{in} and M-$1'_{in}$) and in the interior of the antechamber (V87, L88, V116, V129), shown in spheres in the cross-sectional side view of an α_7-ring (*B*). (*C*) NOEs between the methyl group of residue M1 of the gate (note that the NOESY spectrum was recorded on the WT protein) and methyls of V129 (located close to the α-annulus). (*D*–*H*) Residues showing multiple correlations in the presence of the gates (red) and a single correlation when gates are removed (black).

fact that gates can be either *in* or *out* as well as the potential for different interactions involving the lumen residues with the *in* gates, supporting the results of the PRE study that establish the proximity of these residues to the gate. It is worth noting that peak doubling is also observed for L81δ1 in the context of WT α_7 particles (Fig. 4*H*, red contours), while only a single peak is noted for the L81δ1 methyl in Δ1–12 α_7 (Fig. 4*H*, black contours).

Having identified a general region of the proteasome antechamber that includes residues proximal to the *in* gates, we asked whether it might be possible in certain cases to influence P^{in} values by mutagenesis of the proteasome lumen. Notably, the F91R mutation reduces P^{in} for the PWT gate from 0.96 (ΔG = −1.9 kcal/mol) to 0.74 (ΔG = −0.67 kcal/mol). Fig. 5*A* (circles) shows the results of a titration whereby PWT gate-containing subunits (F91R) and gateless subunits (F91R) are mixed, analogous to the experiments described above. Using model 1, M^{in} = 2 and $P_1^{in} = P_2^{in}$, a best-fitted P^{in} value of 0.74 ± 0.01 is obtained (Fig. 5*A*, red dashed line). The sensitivity of the titration profile to P_i^{in} values is shown in Fig. 5*A* as well, with curves simulated with $0.19 \le P_i^{in} \le 0.96$ (dashed lines). Notably, poor agreement between the experimental profile and those predicted assuming positive cooperativity ($P_1^{in} < P_2^{in}$) (Fig. 5*B*, blue dashed line) or negative cooperativity ($P_1^{in} > P_2^{in}$) (Fig. 5*B*, aqua, yellow and orange dashed lines) is obtained, suggesting that the gates have little interactions in both *out* and *in* positions. As expected, model 2 fits the data equally well as model 1 for the case where M^{in} = 2 and the resulting probabilities are also consistent with a lack of cooperativity between gating elements. Taken together, our fitting results, exploiting a pair of different gating models that make very different assumptions regarding the gating mechanism, and based on experimental data from PWT gates, Y8G/D9G gates and the F91R α_7 mutant provide strong evidence that gating in the *T. acidophilium* proteasome is not cooperative.

Intergate Contacts Are Essential for Proper Function of the 20S CP–11S RP Complex. The titration studies described in this work provide strong evidence that intergate interactions, if present in the naked *T. acidophilium* 20S CP, do not contribute to the energetics of the *in*/*out* gate equilibrium. However, binding of the 11S RP to the 20S CP promotes the CP's peptidase activity by opening the gates (14) and stabilizing the *out* conformation through a cluster of four interacting residues that include Y8 and

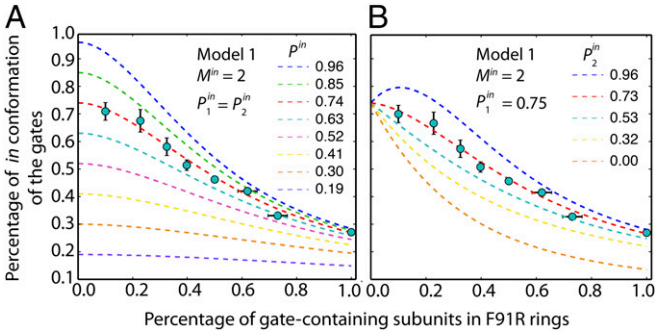

Fig. 5. The F91R mutation has a large effect on gating probabilities. (*A*) Mutation of F91 to R in the antechamber reduces P^{in} from 0.96 ± 0.01 (WT α_7-ring) to 0.74 ± 0.01 (F91R α_7-ring). The corresponding titration curve using the F91R mutant is best fit with $P_1^{in} = P_2^{in} = P^{in} = 0.74 \pm 0.01$ (red dashed line) assuming $M^{in} = 2$ (*Model 1*). Titration curves simulated with P^{in} ranging from 0.96 to 0.19 are shown in colored dashed lines. (*B*) As in *A* but P_1^{in} and P_2^{in} are fit independently, with best fit of $P_1^{in} = 0.75 \pm 0.02$ and $P_2^{in} = 0.73 \pm 0.03$ (red dashed line), along with simulated titration curves using model 1 with $P_1^{in} = 0.75$ and P_2^{in} varied from 0.0 to 0.96. The poor agreement between experimental data and simulated profiles with $P_2^{in} \neq P_1^{in}$ argues strongly that the system is not cooperative.

D9 of the gate, as well as P17 and Y26, and that involve neighboring α-subunits (14) (Fig. 6*A*). The importance of this cluster is underscored by the fact that mutations of these residues have been shown to negatively impact the efficacy of substrate hydrolysis regulated by the PAN complex (38). Previously, we had shown via NMR studies of α_7-rings containing all Y8G/D9G protomers that binding of the 11S RP did not shift the *in*/*out* gate equilibrium and hence did not open the gates, while binding of the 11S RP to WT α_7 generated a completely open structure (23). However, we were not able to unequivocally establish whether the inability to shift the gate equilibrium in the Y8G/D9G α_7-rings was due to the disruption of intergate interactions that would normally form in the complex or simply the result of defects in each gating terminus caused by the mutations. The ability to generate mixed α_7-rings comprising different gates provides a direct route to address this question. α_7-rings were prepared by mixing U-^{2}H, Met-[ε^{13}CH$_3$]–labeled PWT gate-containing subunits (Fig. 6*B*, red sphere) with U-^{2}H Y8G/D9G gate-containing α-protomers (Fig. 6*B*, gray spheres) in a 1:20 molar ratio. The resulting ^{13}C–^{1}H HMQC spectra recorded in the absence (Fig. 6*B*, red contours) and presence (Fig. 6*C*, green contours) of U-^{2}H 11S RP indicate that the 11S RP can indeed bind to an α_7-ring that is largely composed of Y8G/D9G gates (compare green and red peaks for M-1$_{out}$, corresponding to the presence and absence of the 11S RP, respectively, in Fig. 6*C*). Formation of the α_7–11S RP complex is further established by pulsed field gradient diffusion measurements (39) that show a decrease in the diffusion constant from 4.4 ± 0.1 × 10^{-7} to 3.5 ± 0.2 × 10^{-7} cm^2·s^{-1} for α_7 and α_7–11S, respectively (Fig. 6*D*), consistent with predictions based on the program HYDROPRO NMR (40). However, unlike for PWT- or WT-α_7 (23) (Fig. S7), binding of the 11S RP to the mixed α_7-particle described above is not accompanied by a change in the *in*/*out* equilibrium (Fig. 6*C*), as the percentages of *in* gates are essentially independent of 11S (36.3 ± 0.2% and 36.2 ± 0.5% without and with 11S, respectively). These results indicate that interactions between gating residues of adjacent protomers (Fig. 6*A*) are critical for the correct biological response to 11S regulatory particle binding.

Discussion

The proteasome is a key component in controlling cellular proteostasis (41, 42). It carries out its critical functions by regulating the concentrations of proteins in a timely manner and in a way that manages a variety of important biological processes. Although it is established that the 19S RP–20S CP complex plays the dominant role in the degradation of short-lived proteins (43), it is becoming increasingly clear that a large number of protein substrates, estimated to be greater than 20% of cellular proteins (44), can be degraded directly by the naked 20S CP. These substrates are primarily unstructured or contain large unstructured segments and include molecules that play critical roles in cellular functions such as the tumor suppressor p53 (45), the cell cycle regulator p21 (46), and the Parkinson's disease-related protein α-synuclein (47). It is clear that, especially in these cases, the proteasome gates must assume a critical role in controlling which proteins are degraded. Notably, a recent study showed that open-gate mutants of mammalian 20S CPs lead to elevated degradation of many proteins in the cell (~200) and increase cellular resistance to oxidative stress (48). The importance of gating is further underscored in studies where it is estimated that >30% of the proteasomes in mammalian systems are uncapped (49, 50).

In an effort to understand the mechanism of 20S CP gating in detail, we have focused our studies here and in a series of previous papers (22, 23, 30, 33, 35) on the *T. acidophilium* 20S CP. There are a number of advantages of this system for biophysical studies. Unlike proteasome CPs from eukaryotes, the archaeal version contains 14 copies of single α- and β-subunits that can be expressed to high yield. A variety of different constructs can be stably produced (35) including rings of α-protomers, α_7, that are used in this work. Individual subunits can be unfolded and refolded to high yields so that mixed rings can be generated from different protomers that are uniquely labeled.

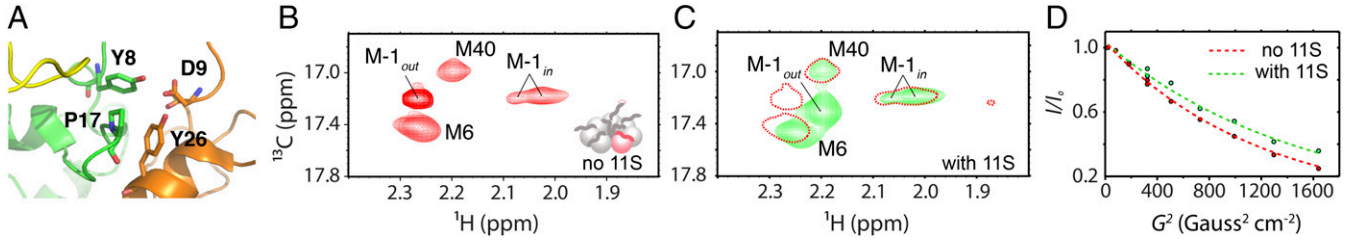

Fig. 6. Interaction between Y8 and D9 from neighboring gates is essential to the gate-opening mechanism of 11S. (*A*) Interaction among a cluster of four conserved residues (Y8, D9, P17, and Y26) on the α-ring stabilizes the open-gate conformation of the proteasome in the 11S-bound state [PDB ID code 1YA7 (14)]. Portions of two neighboring α-subunits are shown in green and orange, and the segment from 11S is shown in yellow. ^{13}C–^{1}H HMQC spectra (800 MHz, 40 °C) of reconstituted α_7-rings (*B*, schematic), consisting of 5% U-^{2}H, Met-[^{13}CH$_3$]–labeled PWT subunits (*B*, red spheres) and 95% U-^{2}H–labeled Y8G/D9G subunits (*B*, gray spheres) in the absence (*B*, red contours, and *C*, red single contour) and presence (*C*, green contours) of 11S. Binding of 11S is indicated by the shift of the *out* peak of M-1 (*C*, M-1$_{out}$) as well as the M6 peak and by the measured diffusion constants (*D*), showing a decrease from (4.36 ± 0.12) × 10^{-7} cm^2·s^{-1} for α_7-rings (*D*, red dashed line) to (3.47 ± 0.16) × 10^{-7} cm^2·s^{-1} for the α_7–11S complex (*D*, green dashed line) (25 °C).

Previous studies have shown that the N-terminal gating residues of the *T. acidophilium* 20S CP are highly dynamic and intrinsically disordered (23). However, they play an important role in regulating substrate hydrolysis rates by existing in either *out* or *in* conformations, leading to a partial occlusion of the α-annulus. On average, two of seven gates reside in the *in* conformation with *in*/*out* lifetimes of several seconds (45 °C). Although macroscopic properties of gating, such as the average number of *in* and *out* gates per ring, could be obtained through studies of α_7-particles composed of a single type of protomer, information about the microscopic properties of the gates such as the intrinsic probability of a gate entering the lumen of the barrel could not be obtained from these bulk measurements, nor could insight be provided that addresses the potential cooperativity of the gating process. Here, by reconstituting α_7-particles using U-^{2}H, Met-[$\varepsilon^{13}CH_3$]–labeled PWT gate-containing protomers and U-^{2}H–labeled gateless protomers in a 1:20 ratio, we have shown that the intrinsic probability of a gate entering the proteasome lumen is very high, ∼95%. By carrying out experiments where the ratio of these protomer types is varied and fitting the resulting titration curve to a pair of statistical models that are derived on the basis of very different assumptions (Fig. 3 *A* and *B* and Fig. S4), we establish that our data are consistent with a noncooperative gating process where only two gates can reside inside the lumen simultaneously and where the probability of entry for each is greater than 95%. Similar experiments using protomers with Y8G/D9G mutations show that three gates can be accommodated, with very high P_i^{in} values, again in a noncooperative manner. The increased M^{in} value in this case is interpreted as resulting from the smaller size of Gly relative to Tyr and Asp that allows an additional gate to penetrate the α-annulus. Finally, a titration experiment using the F91R mutant that reduces P^{in} to 0.74 provides further evidence in support of a lack of gating cooperativity (positive or negative).

The high intrinsic gating probability for the WT α_7-particles (P^{in} = 0.96) could be rationalized qualitatively by interactions between gating residues and hydrophobic amino acids in the interior of the lumen, including V87, L88, F91, V116, and V129. These were quantified by NOE and PRE experiments and mutagenesis, as well as by the doubling of cross-peaks from a number of these residues in ^{13}C–^{1}H HMQC spectra recorded of PWT-α_7 but not in the corresponding spectra of gateless α_7-particles. These interactions are most likely transient, given the highly dynamic nature of the gating residues in the *in* conformation, with squared values of the order parameters for the M-1, M1, and M6 methyl groups less than 0.1 (23).

Notably, peak doubling was also observed for L81δ1, although L81 is not located in the interior of the chamber and is not close to the gate in either of the gate conformations, while only a single peak is noted for the L81δ1 methyl in Δ1–12 α_7. L81 is highly conserved and is located in a region between adjacent α-subunits that binds all known RPs (16). Furthermore, it is connected to the active site of the 20S CP through an allosteric pathway spanning 80 Å that includes antechamber residues V87 and L88 (30). It is of interest to speculate that the peak doubling observed for L81δ1 reflects interactions between the *in*-gate residues and V87 and L88 (see above) that are transmitted to other residues (such as L81) via this pathway (30).

As described above, central to our ability to obtain *in*/*out* gate probabilities and insight into gating cooperativity has been the production of α_7-particles with mixtures of different protomers in which only one protomer type is labeled with NMR active nuclei. This approach holds promise for studies of other molecular machines as well since many of these are also homo-oligomeric and contain gate-like domains. One example is provided by ClpB whose N-terminal domains are thought to play a role in occluding substrate entry (51), or the case of the p97 ATPase where N-terminal motifs bind to substrates or adaptors and play critical roles in the many different functions of this enzyme (52). It will be of interest to see if, like the *T. acidophilium* α-subunit–gating termini, these domains act independently or whether they behave in a cooperative manner.

The present study emphasizes the unique role that solution-based NMR spectroscopy can play in functional studies of biomolecular machines, in particular, in cases involving highly dynamic regions of structure that are of biological importance. The intrinsically disordered nature of the gating residues in the *T. acidophilium* 20S CP makes them difficult to be observed by crystallography or by cryo-electron microscopy where the small size of the gates (10–15 residues) and the multiplicity of conformers challenges identification and classification of states. A combination of NMR and other powerful methods that generate high-resolution images of large complexes appears to be a promising avenue for describing both structure and dynamics, leading to a quantitative description of how function is generated.

Materials and Methods

All NMR data were acquired on a pair of 600-MHz Varian spectrometers as well as 600- and 800-MHz Bruker AVANCE III HD spectrometers. Three of the four instruments were equipped with cryogenically cooled triple-resonance probes.

^{13}C–^{1}H HMQC spectra were acquired at 50 °C (α_7-rings) or 40 °C (α_7–11S complex and α_7-rings compared with those in the complex). For Met methyl-only–labeled samples, HMQC spectra were recorded with an interscan delay of 1.5 s, offsets of 2.13 ppm (^{1}H) and 17.0 ppm (^{13}C), and acquisition times of 53 and 64 ms in the t_1 and t_2 dimensions, respectively, while for ILVM methyl-labeled samples offsets of 1.0 ppm (^{1}H) and 19.0 ppm (^{13}C) and acquisition times of 18 (t_1) and 64 ms (t_2) were used. Intensities of the *in* and *out* conformations of M-1 were obtained via "box sums" implemented with NMRGlue (53), and corrected for differential ^{1}H R_2 relaxation during delays in the HMQC pulse scheme, as described in *Supporting Information* (33). Three-dimensional ^{13}C-edited nuclear Overhauser effect spectroscopy (NOESY) experiments were recorded on ILVM methyl-labeled WT α_7-rings, 50 °C, 800 MHz, using a methyl-TROSY–based pulse scheme of the form, $^{13}C(t_1)$-NOE-$^{13}C(t_2)$-$^1H(t_3)$ (sequence available upon request), with a mixing time of 300 ms.

A description of the expression, purification, and reconstitution of α_7-rings, further details of the NMR experiments, and a discussion of the fitting models used are given in *Supporting Information*.

ACKNOWLEDGMENTS. We thank A. Sekhar for a critical reading of the manuscript, and A. Velyvis for valuable discussions. This work was supported through a grant from the Canadian Institutes of Health Research. L.E.K. holds a Canada Research Chair in Biochemistry.

1. Chen B, Retzlaff M, Roos T, Frydman J (2011) Cellular strategies of protein quality control. *Cold Spring Harb Perspect Biol* 3:a004374.
2. Balch WE, Morimoto RI, Dillin A, Kelly JW (2008) Adapting proteostasis for disease intervention. *Science* 319:916–919.
3. Bhattacharyya S, Yu H, Mim C, Matouschek A (2014) Regulated protein turnover: Snapshots of the proteasome in action. *Nat Rev Mol Cell Biol* 15:122–133.
4. Marques AJ, Palanimurugan R, Matias AC, Ramos PC, Dohmen RJ (2009) Catalytic mechanism and assembly of the proteasome. *Chem Rev* 109:1509–1536.
5. Finley D, Chen X, Walters KJ (2016) Gates, channels, and switches: Elements of the proteasome machine. *Trends Biochem Sci* 41:77–93.
6. Tomko RJ, Jr, Hochstrasser M (2013) Molecular architecture and assembly of the eukaryotic proteasome. *Annu Rev Biochem* 82:415–445.
7. Kish-Trier E, Hill CP (2013) Structural biology of the proteasome. *Annu Rev Biophys* 42:29–49.
8. Manasanch EE, Orlowski RZ (2017) Proteasome inhibitors in cancer therapy. *Nat Rev Clin Oncol* 14:417–433.
9. Kisselev AF, Goldberg AL (2001) Proteasome inhibitors: From research tools to drug candidates. *Chem Biol* 8:739–758.
10. Adams J (2004) The proteasome: A suitable antineoplastic target. *Nat Rev Cancer* 4:349–360.
11. Löwe J, et al. (1995) Crystal structure of the 20S proteasome from the archaeon *T. acidophilum* at 3.4 Å resolution. *Science* 268:533–539.
12. Groll M, et al. (1997) Structure of 20S proteasome from yeast at 2.4 Å resolution. *Nature* 386:463–471.
13. Unno M, et al. (2002) The structure of the mammalian 20S proteasome at 2.75 Å resolution. *Structure* 10:609–618.
14. Förster A, Masters EI, Whitby FG, Robinson H, Hill CP (2005) The 1.9 Å structure of a proteasome-11S activator complex and implications for proteasome-PAN/PA700 interactions. *Mol Cell* 18:589–599.

15. Li X, et al. (2013) Electron counting and beam-induced motion correction enable near-atomic-resolution single-particle cryo-EM. *Nat Methods* 10:584–590.
16. Rabl J, et al. (2008) Mechanism of gate opening in the 20S proteasome by the proteasomal ATPases. *Mol Cell* 30:360–368.
17. Yu Y, et al. (2010) Interactions of PAN's C-termini with archaeal 20S proteasome and implications for the eukaryotic proteasome-ATPase interactions. *EMBO J* 29:692–702.
18. Huang X, Luan B, Wu J, Shi Y (2016) An atomic structure of the human 26S proteasome. *Nat Struct Mol Biol* 23:778–785.
19. Schweitzer A, et al. (2016) Structure of the human 26S proteasome at a resolution of 3.9 Å. *Proc Natl Acad Sci USA* 113:7816–7821.
20. Dambacher CM, Worden EJ, Herzik MA, Martin A, Lander GC (2016) Atomic structure of the 26S proteasome lid reveals the mechanism of deubiquitinase inhibition. *Elife* 5: e13027.
21. Chen S, et al. (2016) Structural basis for dynamic regulation of the human 26S proteasome. *Proc Natl Acad Sci USA* 113:12991–12996.
22. Ruschak AM, Religa TL, Breuer S, Witt S, Kay LE (2010) The proteasome antechamber maintains substrates in an unfolded state. *Nature* 467:868–871.
23. Religa TL, Sprangers R, Kay LE (2010) Dynamic regulation of archaeal proteasome gate opening as studied by TROSY NMR. *Science* 328:98–102.
24. Bajorek M, Finley D, Glickman MH (2003) Proteasome disassembly and down-regulation is correlated with viability during stationary phase. *Curr Biol* 13:1140–1144.
25. Forouzan D, et al. (2012) The archaeal proteasome is regulated by a network of AAA ATPases. *J Biol Chem* 287:39254–39262.
26. Barthelme D, Chen JZ, Grabenstatter J, Baker TA, Sauer RT (2014) Architecture and assembly of the archaeal Cdc48*20S proteasome. *Proc Natl Acad Sci USA* 111: E1687–E1694.
27. Bolten M, et al. (2016) Structural analysis of the bacterial proteasome activator Bpa in complex with the 20S proteasome. *Structure* 24:2138–2151.
28. Schmidt M, et al. (2005) The HEAT repeat protein Blm10 regulates the yeast proteasome by capping the core particle. *Nat Struct Mol Biol* 12:294–303.
29. Stadtmueller BM, Hill CP (2011) Proteasome activators. *Mol Cell* 41:8–19.
30. Ruschak AM, Kay LE (2012) Proteasome allostery as a population shift between interchanging conformers. *Proc Natl Acad Sci USA* 109:E3454–E3462.
31. Tugarinov V, Hwang PM, Ollerenshaw JE, Kay LE (2003) Cross-correlated relaxation enhanced ^{1}H–^{13}C NMR spectroscopy of methyl groups in very high molecular weight proteins and protein complexes. *J Am Chem Soc* 125:10420–10428.
32. Rosenzweig R, Kay LE (2014) Bringing dynamic molecular machines into focus by methyl-TROSY NMR. *Annu Rev Biochem* 83:291–315.
33. Latham MP, Sekhar A, Kay LE (2014) Understanding the mechanism of proteasome 20S core particle gating. *Proc Natl Acad Sci USA* 111:5532–5537.
34. Battiste JL, Wagner G (2000) Utilization of site-directed spin labeling and high-resolution heteronuclear nuclear magnetic resonance for global fold determination of large proteins with limited nuclear overhauser effect data. *Biochemistry* 39: 5355–5365.
35. Sprangers R, Kay LE (2007) Quantitative dynamics and binding studies of the 20S proteasome by NMR. *Nature* 445:618–622.
36. Liu CW, Corboy MJ, DeMartino GN, Thomas PJ (2003) Endoproteolytic activity of the proteasome. *Science* 299:408–411.
37. Häckel M, Hinz HJ, Hedwig GR (1999) Partial molar volumes of proteins: Amino acid side-chain contributions derived from the partial molar volumes of some tripeptides over the temperature range 10–90° C. *Biophys Chem* 82:35–50.
38. Förster A, Whitby FG, Hill CP (2003) The pore of activated 20S proteasomes has an ordered 7-fold symmetric conformation. *EMBO J* 22:4356–4364.
39. Choy WY, et al. (2002) Distribution of molecular size within an unfolded state ensemble using small-angle X-ray scattering and pulse field gradient NMR techniques. *J Mol Biol* 316:101–112.
40. Ortega A, Amorós D, García de la Torre J (2011) Prediction of hydrodynamic and other solution properties of rigid proteins from atomic- and residue-level models. *Biophys J* 101:892–898.
41. Dikic I (2017) Proteasomal and autophagy degradation systems. *Annu Rev Biochem* 86:193–224.
42. Bajorek M, Glickman MH (2004) Keepers at the final gates: Regulatory complexes and gating of the proteasome channel. *Cell Mol Life Sci* 61:1579–1588.
43. Ben-Nissan G, Sharon M (2014) Regulating the 20S proteasome ubiquitin-independent degradation pathway. *Biomolecules* 4:862–884.
44. Baugh JM, Viktorova EG, Pilipenko EV (2009) Proteasomes can degrade a significant proportion of cellular proteins independent of ubiquitination. *J Mol Biol* 386: 814–827.
45. Asher G, Tsvetkov P, Kahana C (2005) A mechanism of proteasomal degradation of the tumor suppressors p53 and p73. *Genes Dev* 19:316–321.
46. Li X, et al. (2007) Ubiquitin- and ATP-independent proteolytic turnover of p21 by the REGgamma-proteasome pathway. *Mol Cell* 26:831–842.
47. Tofaris GK, Layfield R, Spillantini MG (2001) alpha-Synuclein metabolism and aggregation is linked to ubiquitin-independent degradation by the proteasome. *FEBS Lett* 509:22–26.
48. Choi WH, et al. (2016) Open-gate mutants of the mammalian proteasome show enhanced ubiquitin-conjugate degradation. *Nat Commun* 7:10963.
49. Fabre B, et al. (2013) Subcellular distribution and dynamics of active proteasome complexes unraveled by a workflow combining in vivo complex cross-linking and quantitative proteomics. *Mol Cell Proteomics* 12:687–699.
50. Tanahashi N, et al. (2000) Hybrid proteasomes. Induction by interferon-gamma and contribution to ATP-dependent proteolysis. *J Biol Chem* 275:14336–14345.
51. Rosenzweig R, et al. (2015) ClpB N-terminal domain plays a regulatory role in protein disaggregation. *Proc Natl Acad Sci USA* 112:E6872–E6881.
52. Schuetz AK, Kay LE (2016) A dynamic molecular basis for malfunction in disease mutants of p97/VCP. *Elife* 5:e20143.
53. Helmus JJ, Jaroniec CP (2013) Nmrglue: An open source Python package for the analysis of multidimensional NMR data. *J Biomol NMR* 55:355–367.
54. Velyvis A, Ruschak AM, Kay LE (2012) An economical method for production of ^{2}H, $^{13}CH_3$-threonine for solution NMR studies of large protein complexes: Application to the 670 kDa proteasome. *PLoS One* 7:e43725.
55. Gibson DG, et al. (2009) Enzymatic assembly of DNA molecules up to several hundred kilobases. *Nat Methods* 6:343–345.
56. Tugarinov V, Kanelis V, Kay LE (2006) Isotope labeling strategies for the study of high-molecular-weight proteins by solution NMR spectroscopy. *Nat Protoc* 1:749–754.
57. Huang C, Rossi P, Saio T, Kalodimos CG (2016) Structural basis for the antifolding activity of a molecular chaperone. *Nature* 537:202–206.
58. Delaglio F, et al. (1995) NMRPipe: A multidimensional spectral processing system based on UNIX pipes. *J Biomol NMR* 6:277–293.
59. Goddard TD, Kneller DG (2008) *SPARKY 3* (University of California, San Francisco).
60. Press WH, Flannery BP, Teukolsky SA, Vetterling WT (1998) *Numerical Recipes in C* (Cambridge Univ Press, Cambridge, UK).